Doctoral Thesis

CFD MODEL OF VEHICLE CONDENSER

University of Pardubice
Faculty of Transport Engineering

Ing. Michal Schmid

Pardubice, Month Dayth, 2023

Department of Mechanics, Materials and Machine Parts

Supervisor:
doc. Ing. Petr Tomek, Ph.D.
University of Pardubice, Faculty of Transport Engineering
Supervisor specialist:
RNDr. Mgr. Václav Mácha , Ph.D.
Institute of Mathematics of the Czech Academy of Sciences

Programme of Study:
P3710 Technique and Technology in Transport and Communications
Branch of Study:
3706V005 - Transport Means and Infrastructure
Supervisors:
doc. Ing. Petr Tomek, Ph.D.
RNDr. Mgr. Václav Mácha , Ph.D.
Dissertation Title:
CFD model of vehicle condenser
The doctoral dissertation has arisen at the supervising:
Educational and Research Centre in Transport (ERCT)

Declaration of authorship

I hereby declare:
This thesis was prepared individually. All the literary sources and the information I used in the thesis are listed in the bibliography.
I was familiar with the fact that rights and obligations arising from the Act No. 121/2000 Coll., the Copyright Act, apply to my thesis, especially with the fact that the University of Pardubice has the right to enter into a license agreement for the use of this thesis as a school work pursuant to § 60, Section 1 of the Copyright Act, and the fact that should this thesis be used by me or should a license be granted for the use to another entity, the University of Pardubice is authorized to claim from me a reasonable contribution to cover the costs incurred during the making of the thesis, according to the circumstances up to the actual amount thereof.
I agree with the reference-only disclosure of my thesis in the University Library.

Location, date

_____

Name

Abstract

The AC condenser plays a vital role in HVAC systems (Heating Ventilating Air Conditions). In vehicles, it is typically located within a cooling pack, alongside other heat exchangers. The dissipation of heat from the AC condenser directly affects surrounding components. Therefore, accurate modeling of heat transfer between the refrigerant and air is crucial for vehicle development, especially nowadays for battery electric vehicles.

The proposed model enhances the spatial distribution of heat transfer, resulting in improved air temperature predictions. The proposed model is based on the well-known and established $\epsilon - NTU$ approach and iterative takes into account the appropriate relation according to the refrigerant phase during the condensation process occurring in the condenser. Additionally, the approach reduces the amount of required input data and relies on directly measured condenser characteristics, leading to more generic approach.

In the thesis, a dedicated test equipment was developed for input data measurement and model verification. The proposed model was tested under two distinct conditions and compared with measurements. The model exhibited good agreement with the measurements in predicting refrigerant inlet and outlet temperatures, as well as relatively good agreement in air outlet temperature prediction. Furthermore, additional development tasks were identified as well.

Keywords:
AC Condenser, CFD, Heat Transfer, Measurement

Acknowledgements

I am deeply thankful to my supervisors prof. Ing. Petr Paščenko, Ph.D., doc. Ing. Petr Tomek, Ph.D. and RNDr. Mgr. Václav Mácha, Ph.D.,and my family, for their guidance, invaluable suggestions, technical expertise, and moral support.

Contents

Nomenclature

AC	Air Conditioning
CFD	Computational Fluid Dynamics
HTX	Heat Exchanger
$HVAC$	Heating, Ventilating, and Air Conditioning

α	Convective heat transfer coefficient	$(W/(m^2K))$
χ	Vapor/Refrigerant quality	$(-)$
Δ	Difference	$(-)$
$\dot{m}$	Mass flow rate	(kg/s)
$\dot{Q}$	Heat transfer rate	(W)
ϵ	Effectiveness	$(-)$
λ	Thermal conductivity	$(W/(mK))$
A	Area, Heat transfer area, Cell surface area	(m^2)
C	Heat capacity	(W/K)
c_p	Specific heat capacity at constant pressure	$(J/(kgK))$
Cr	Heat capacity ratio	$(-)$
dx, dy, dz	Cell size in x,y,z direction	(m)
G_i	Geometrical Parameter	$(m; -)$
h	Specific enthalpy	(J/kg)
N	Cell count	$(-)$
NTU	Number of transfer unit	$(-)$
p	Static pressure	(Pa)

$R_{specific}$	Specific gas constant	$(J/(kgK))$
T	Temperature	(K)
U	Overall heat transfer coefficient	$(W/(m^2K))$
u	Velocity magnitude	(m/s)
Un	Uncertainty	$(-)$
V	Volume	(m^3)
$Xcells, Ycells, Zcells$	Cell count in x,y,z direction	$(-)$

Subscripts

aux	Auxiliary fluid
ave	Average
$global$	Heat exchanger domain level
i, j, k	x,y,z axis index
in	Inlet
$local$	Local level (macro, cell)
m	Arithmetic mean
max	Maximum
min	Minimum
n	Sample point
out	Outlet
$prim$	Primary fluid
$table$	Input table level

1 Introduction

Nowadays, virtual prototyping has become an integral part of modern vehicle development. It encompasses a wide range of activities, including numerical simulations, drawings, and product lifecycle management. The simulations themselves encompass various physical phenomena, ranging from electromagnetism, fluid dynamics, and thermal dynamics to structural analyses. The prevalent numerical methods used in modern simulations are the Finite Volume Method (FVM) and the Finite Element Method (FEM). However, other numerical approaches such as Lattice Boltzmann or Smooth Particle Hydrodynamics are gaining popularity. In recent years, computational resources have significantly expanded, enabling the creation of comprehensive numerical models that utilize hundreds or thousands of CPUs (Central Processing Units) per simulation. This utilization of High-Performance Computing (HPC) is not limited to CPUs alone; graphics cards are also being employed in HPC applications. From an engineering perspective, virtual prototyping allows for a reduction in the number of physical prototypes and measurements required. Furthermore, simulation plays a crucial role in vehicle optimization and design exploration. As a result, virtual prototyping is indispensable in the current automotive industry due to increasingly stringent emissions regulations and other vehicle design requirements. Consequently, these demands have led to higher requirements for simulation accuracy, computational time reduction, and other factors. Computational Fluid Dynamics (CFD) is particularly vital in the development of vehicle thermal management and overall vehicle design, such as external aerodynamics. The accuracy of simulations is even more critical for modern battery electric vehicles (BEVs) due to their lower energy reserves compared to conventional combustion engine (ICE) vehicles. Each watt of energy must be carefully considered to extend the vehicle's range. Additionally, the heat dissipation within the system is lower in BEVs, leading to lower system temperatures. Therefore, accurately capturing small temperature differences becomes essential in this context.

One of the crucial components in vehicle thermal management is the HVAC (Heating, Ventilating, and Air Conditioning) system. The HVAC system plays a crucial role in ensuring cabin comfort, occupant safety, as well as the cooling of the engine or battery pack in the case of BEVs. The significance of the HVAC system in the context of vehicle electrification is extensively discussed in König et al. (2022). The HVAC unit typically comprises various elements, including a cabin heater, AC (Air Conditioning) evaporator, condenser, ducting, filters, blower, compressor, and others. As a major contributor to vehicle fuel or electric energy consumption, optimizing the energy efficiency of the HVAC system holds significant importance in modern vehicle development. Generally, the heat generated by the vehicle, such as the cabin and the battery pack, dissipates into the surrounding air within the studied heat exchangers.

In modern vehicles, various heat exchangers (HTX) are integrated primarily for the purpose of dissipating heat into the ambient air. Examples of these HTX include the engine coolant HTX (radiator), Charged Air Cooler (CAC), as well as coolers for steering, transition oil, fuel, and the aforementioned AC condenser. These HTX are typically combined with a cooling fan and shroud to form a so-called cooling pack. Consequently, each HTX has an impact on the others within this assembly. Computational Fluid Dynamics (CFD) simulations focused on this area are commonly referred to as under bonnet/underhood thermal management (UTHM) or front-end simulations. The CFD modeling of HTX not only affects the prediction of coolant, oil, and fuel temperatures (auxiliary fluids) but also influences other under-bonnet components (exhaust, battery, brackets, filters, etc.) due to the airflow heating. The accurate prediction of airflow rate and fluid temperatures relies directly on the proper modeling of HTX heat transfer.

This thesis specifically focuses on enhancing the heat transfer model of the AC condenser within a comprehensive underhood CFD simulation of a full vehicle. The objective is to improve prediction of heat dissipation from the AC condenser. The proposed model enhancement aims to accurately capture the thermodynamic characteristics of each section of the AC condenser, considering both phase change and single-phase regions. The appropriate heat transfer model should be implemented based on the operating conditions and boundary conditions of the AC condenser. By improving the 1D AC condenser model, the accuracy of airflow rate and temperature predictions in full vehicle CFD simulations should be increased as well. The standard physical measurements of HTX need to be modified to obtain suitable input data for the suggested numerical model. Furthermore, the proposed model and measurement technique are more general compared to existing approaches for AC condenser modeling. Additionally, a verification measurement is conducted to validate and demonstrate the benefits of the developed AC condenser model.

The initial thesis sections discuss the calculations, modeling, and measurement related to the AC condensers. Furthermore, it suggests objectives based on current state-of-the-art research. The thesis Sections 3, 4.1, 4.2, 4.3, and 4.4 presents the suggested and developed AC condenser model. In Section 5, the thesis describes the measurement devices and test equipment developed for obtaining input data for the model and verifying model accuracy. The subsequent part of the thesis presents the results of the measurements and the calculations performed using the AC condenser model. Finally, the results are compared, discussed, and summarized in the conclusions. The conclusions also outline future steps based on the findings and conclusions of the thesis.

2 Objectives

The primary aim of this research is to enhance the accuracy of AC condenser modeling within a complex full-vehicle 3D CFD simulation, where implementing a detailed heat exchanger model is not feasible. The proposed model seeks to improve the prediction of local heat transfer between the refrigerant and cooling air within the AC condenser. By achieving enhanced heat transfer prediction, the accuracy of airflow simulation should be improved as well, leading to more precise predictions for other vehicle components and fluids, such as coolant and oil. Moreover, the proposed model and measurement approach simplify and generalize the current procedures used for calculating local heat transfer.
The enhancement of the proposed model relies on accurately defining local heat transfer based on the phase or quality of the refrigerant, similar to the approaches adopted by other researchers. However, unlike the current 1D AC condenser calculation methods, which rely on the estimation of convective heat transfer coefficients, the suggested model directly measures the overall heat transfer coefficient. This integration and modification of conventional 3D CFD methods and the latest 1D AC condenser models result in a more comprehensive approach.
Consequently, the measurement of the overall heat transfer coefficient in the suggested model combines and modifies the methodologies used for single-phase heat exchangers and phase change heat exchangers. The gathering of input data for the suggested AC condenser model is expected to be more general and applicable compared to the current state-of-the-art approaches.
By incorporating these advancements, the proposed model aims to improve the accuracy and generalizability of AC condenser modeling, enabling more precise predictions of heat transfer in various refrigerant phases and enhancing the overall performance of the system.
To successfully achieve the aforementioned objectives, several critical tasks need to be accomplished. These key tasks are listed below:

- **Propose the AC condenser model**
  The model should be able to capture local refrigerant quality and select appropriate heat transfer (single vs. dual-phase).
- **Create single-phase HTX calculation algorithm**
  Verify model via comparing with CFD code from
- **Create HTX calculation algorithm including phase change**
- **Test equipment development**
- **Experimental verification**

3 Suggested Model Philosophy

The proposed model integrates the implementation of the $\epsilon - NTU$ approach used in *Ansys Fluent* with the recent advancements made to 1D AC condenser models. Consequently, it requires modification of standard input data ($Q - Table$) measurement.
The primary concept behind the suggested and developed model is the incorporation of the spatial distribution of the $\epsilon - NTU$ relationship to account for the refrigerant phase in an AC condenser. Figure 1 (a) Nozicka (2008) illustrates a temperature-entropy and pressure-enthalpy (T-s and p-h) diagram with an AC circuit. The highlighted section between points 2 and 3 refers to the AC condenser. A schematic representation of the refrigerant flow within the AC condenser is shown in Figure 1 (b), highlighting the relevant sections. The red-marked region indicates the gas phase of the refrigerant. At the saturation temperature denoted as $2''$ in the diagram, a phase change occurs, and the refrigerant transition into a dual-phase state starts, represented by the orange color. The $\epsilon - NTU$ relationship needs to be modified accordingly, utilizing the dual-phase Equation 2 Incropera et al. (2011), Liang et al. (2015). Once the refrigerant dissipates its latent heat into the surrounding air, the condensation process is completed, and it fully transforms into a liquid phase (blue region). This blue section is referred to as overcooling. Consequently, the $\epsilon - NTU$ relationship should revert to Equation 1 Incropera et al. (2011), employing liquid input characteristic data ($Q - Table$). Within each section (red, orange, and blue), specific measured $Q - Tables$ for overall heat transfer should be utilized to accurately characterize the heat transfer process.
The proposed model follows an iterative approach similar to the works of Rice and Sand (1990), Admiraal and Bullard (1993), or Bansal and Purkayastha (1998). Within the same section, it was mentioned that Pervaiz et al. (1997) implemented a spatial distribution of heat transfer coefficient in the *Simcenter* $STAR - CCM+$ model. Additionally, Jha and Shaik (2016) employed a similar approach using the *Gamma Technologies* $GT - SUITE\ COOL3D$ model Gamma Technologies (2014). However, all these models rely on convective heat transfer coefficients obtained from literature, specimen measurements, or fitted correlation equations (fitting to the whole HTX measurement).
The proposed method directly measures the overall heat transfer coefficient (respectively the $Q - table$), which encompasses various heat transfer mechanisms such as tube conduction, phase-change convection, and air-side convection etc. This approach effectively reduces the number of required input parameters, as demonstrated in Figure 2.

$$\epsilon = 1 - exp[-\frac{NTU^{0.22}}{C_r}(1 - e^{-C_r NTU^{0.78}})] \tag{1}$$

$$\epsilon = 1 - exp(-NTU) \tag{2}$$

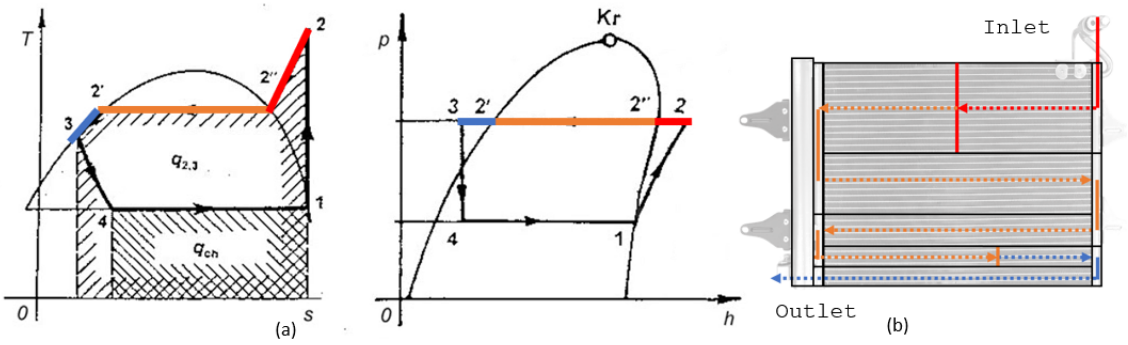

Figure 1: (a) T-s and p-s diagrams Nozicka (2008); AC condenser sections (b)

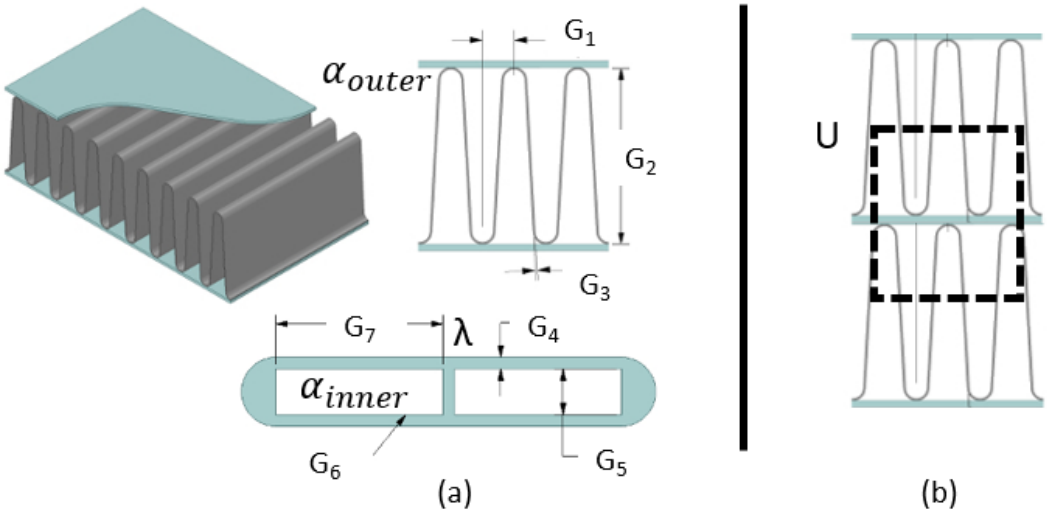

Figure 2: (a) *Gamma Technologies GT – SUITE COOL3D* model inputs Gamma Technologies (2014); suggested model input (b)

4 Model Description

4.1 Computational Domain and Discretization

The computational domain, shown in Figure 3 (a), represents an AC condenser in the standard Cartesian coordinate system for vehicles J902 (2011). The Cartesian axis indexing and the structural mesh of cell volumes are illustrated in Figure 3 (b). The domain (simple block) is discretized using a uniform division with a constant interval. Consequently, each cell (control volume) has identical size and an equal distance between the centroids of adjacent cells. In Figure 3 (b), an example cell is shaded, with the points representing the cell centroids. The dimensions of each cell are defined as dx, dy, and dz. It is important to note that the cell centroid represents a simple 1D element, wherein the values denoting the cell volume are calculated and stored.

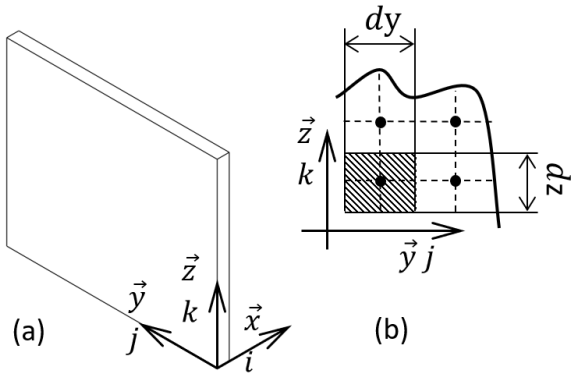

Figure 3: Computational domain (a) and mesh details (b)

4.2 Mass Flow Rate

The suggested condenser model focuses solely on predicting heat transfer and does not simulate fluid flow. Therefore, the mass flow rates of the fluids are considered as boundary conditions based on the measured data. However, it is possible to couple or integrate the suggested condenser model with a 3D CFD code, where the fluid flow can be simulated. This would allow for a more comprehensive analysis of the condenser performance by considering the simulated mass flow rates.

4.2.1 Primary Fluid Flow

The primary flow, which corresponds to the airflow, is considered a measured boundary condition and is obtained from the test device described in Section 5.2. The device measures the magnitude of the airflow velocity and the temperature in the direction parallel to the heat exchanger surface (the x direction, as defined in Section 3).

To calculate the mass flow rate of the airflow, the ideal gas law for dry air (Nozicka (2008)), the measured ambient pressure, and the airflow frontal area are utilized. The air mass flow rate is determined by multiplying the measured velocity magnitude by the airflow frontal area, while assuming a negligible pressure difference between the ambient pressure and the pressure at the inlet surface of the AC condenser.
The uniformity of airflow distribution plays a significant role in the performance of the heat exchanger. More in-depth analysis on the importance of airflow uniformity distribution can be found in Moradi et al. (2020) and Schmid et al. (2021).

$$\dot{m}_{cell} = \frac{p_{ambient}}{R_{specific} \cdot T_{cell}} A_{cell} \cdot u_{i\_cell} \tag{3}$$

4.2.2 Auxiliary Fluid Flow

The refrigerant fluid flow is modeled as a one-dimensional tube flow in the direction of the passes (i.e., through the micro-channel tubes). The mass flow rate of the refrigerant liquid at the AC condenser inlet is prescribed based on the measured value obtained from the experimental data.
Figure 4 illustrates the distribution of the auxiliary fluid (refrigerant) flow between the passes. Equation 4 is used to calculate the flow rate for each computational cell. The defined refrigerant flow rate is divided equally among the cells within the cross-sectional area of a particular pass.

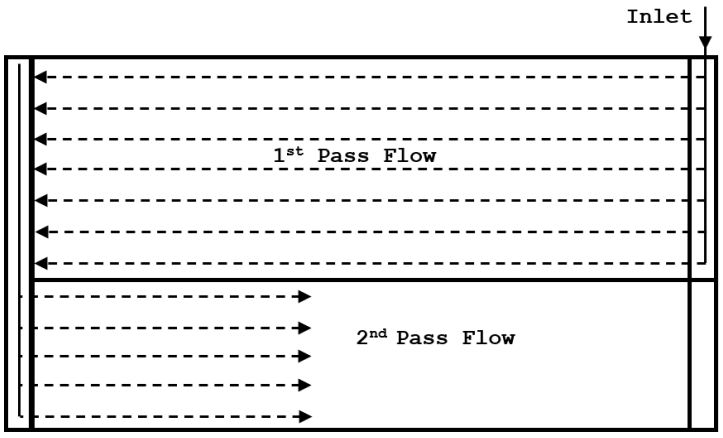

Figure 4: The refrigerant flow distribution scheme

$$\dot{m}_{cell} = \frac{\dot{m}_{aux}}{[Xcells \cdot Zcells]_{Pass}} \tag{4}$$

The distribution of flow within each pass is assumed to be uniform among the parallel tubes. This assumption is based on the Bernoulli equation (Nozicka (2008)). However, in real AC condensers and cross-flow heat exchangers in general, the flow distribution

within the pass tubes can be nonuniform due to three-dimensional effects. The uniformity of the auxiliary fluid flow is an important design parameter in heat exchangers and is balanced against pressure restrictions Zou and Hrnjak (2014). The uniformity of flow is influenced by factors such as tank and tube shape, fluid properties, and mass flow rate. The uniformity of the refrigerant flow in the evaluated condenser is deemed valid based on the geometry of the tanks and tubes, particularly the size ratio between these components. This conclusion is supported by studies such as Minqiang et al. (2009), Mohammadi et al. (2013), Pistoresi et al. (2015), and Wei et al. (2015). However, in the case of nonuniform flow distribution, an alternative approach such as the *Dual Cell* or *Dual Stream* method, applied in Pervaiz et al. (1997), could be employed. Nonetheless, the proposed heat transfer approach remains unchanged.

4.3 Heat Transfer Model

Heat transfer between primary (air) and auxiliary (refrigerant) fluid in the AC condenser is modeled by $\epsilon - NTU$ approach as discussed in Sections 2 and 3. This approach assumes that both fluids are unmixed, meaning that heat transfer occurs only in one direction parallel to the airflow. This assumption is based on the thermodynamic definition of unmixed fluids Taborek (1983). Additionally, it is assumed that the specific heat capacity and density of the fluids are constant, based on the average temperature. This assumption simplifies the calculations and is commonly used in heat transfer analysis.

The schematic for obtaining the NTU value from measured data (represented by the $Q - Table$) is shown in Figure 5. In this measurement process, multiple flow rates of fluids are typically tested in order to gather a range of heat exchanger characteristic data. During the measurement, the inlet temperature for each fluid is kept constant. For the suggested model, it is necessary to measure the $Q-Table$ for each phase of the refrigerant. This means that the heat transfer performance needs to be evaluated separately for both the single-phase and dual-phase regions of the AC condenser.

The first step in the calculation is to determine the heat exchanger efficiency (ϵ) using Equation 8 Kays and London (1984). Once the efficiency is known, the corresponding NTU value can be calculated using an appropriate $\epsilon - NTU$ relationship. For cases where there is no phase change in the measured data, Equation 1 Incropera et al. (2011) is used. On the other hand, for cases involving phase change, Equation 2 Incropera et al. (2011) is employed. It is important to note that when expressing NTU using Equation 1 Incropera et al. (2011), an iterative approach is required. The developed approach utilizes the Newton-Raphson iterative method, which is similar to the implementation in $AnsysFluent$.

Once the NTU values are determined for the entire heat exchanger, the next step is to evaluate the operating point for each individual cell within the heat exchanger. In the

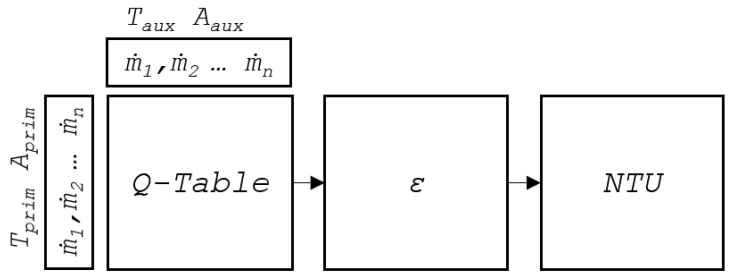

Figure 5: Measured data processing workflow

suggested model, where constant inlet conditions are assumed, the operating point for each cell is calculated only at the beginning of the simulation, as described in Section 4.4. In the case of changing flow conditions, such as varying inlet temperatures or flow rates, the operating point for each cell would need to be calculated iteratively. However, in the suggested model with constant inlet conditions, this iterative calculation is not necessary, and the operating points can be determined at the start of the simulation based on the initial conditions. The operating point for each cell within the heat exchanger is determined using the following expressions. Firstly, the mass flow rate throughout the cell is scaled to the entire dimension of the heat exchanger, resulting in the *global* flow rate, as defined in Equation 9 Fluent (2009). This global flow rate is used to interpolate the corresponding *global NTU* value for each cell from the *NTU* table, using linear interpolation. Based on the *global NTU* value, the *local NTU* value for each cell is defined using Equation 10, following a similar approach as in Fluent (2009). The efficiency of each cell is then calculated based on the local *NTU* value, utilizing the relations provided in Equation 1 Incropera et al. (2011) for non-phase-change conditions, and Equation 2 Incropera et al. (2011) for phase-change conditions. Finally, the heat dissipated by each cell is determined using Equation 7 Incropera et al. (2011) or for phase-change Equation 6 Liang et al. (2015), and the outlet temperatures are calculated using Equation 5 Incropera et al. (2011). These expressions allow for the evaluation of the heat transfer characteristics and outlet temperatures at the cell level within the heat exchanger.

$$\dot{Q}_{local} = \dot{m} c_p \Delta T \tag{5}$$

$$\dot{Q} = \epsilon C_{min}(h_{in,aux} - h_{in,prim}) \tag{6}$$

$$\dot{Q}_{local} = \epsilon_{local} C_{min,local}(T_{in,aux} - T_{in,prim}) \tag{7}$$

$$\epsilon = \frac{\dot{Q}}{\dot{Q_{max}}} = \frac{\dot{Q}}{C_{mins}(T_{in,aux} - T_{in,prim})} \tag{8}$$

$$\dot{m}_{cell}^{global} = \dot{m}_{cell} \frac{A_{Q-Table}}{A_{cell}} \tag{9}$$

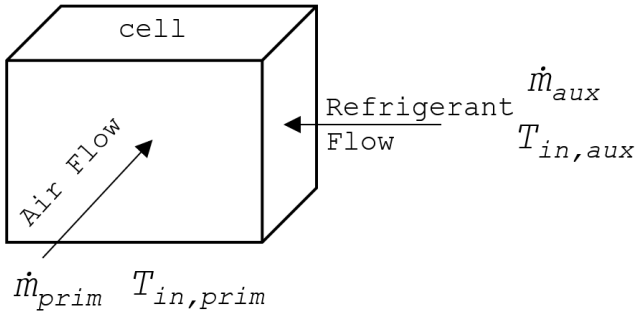

Figure 6: Computational cell flow scheme

$$NTU_{cell}^{local} = NTU_{cell}^{global} \frac{V_{cell} C_{min,global}}{V_{global} C_{min,cell}} \tag{10}$$

4.3.1 Tanks' Flow Mixing

The assumption of ideal mixing inside the tanks of the AC condenser, and with considered uniform mass flow within the HTX core, leads to the assumption of uniform outlet temperatures from the tanks (Section 4). To calculate the uniform outlet temperature or enthalpy from the tanks, the average of the inlet temperature or enthalpy of the tanks is taken. Similarly, the refrigerant phase, specifically the quality χ, is calculated based on the average inlet values for each tank. The refrigerant vapor quality χ ranges from 0 to 1 and is generally defined by Equation 11 and illustrated in Figure 7 Nozicka (2008). However, in the AC condenser model, the vapor quality χ is not treated as a continuous parameter, but rather as discrete ranges/values defined in Equation 12. Based on the value of χ, the appropriate heat transfer calculation is applied in the model.

$$\chi = \frac{m_{vapour}}{m_{vapour} + m_{liquid}} \tag{11}$$

$$Q - Table = \begin{cases} Liquid\ Phase, & \text{if } \chi = 0. \\ DualPhase, & \text{if } 0 < \chi < 1. \\ GasPhase, & \text{if } \chi = 1. \end{cases} \tag{12}$$

4.4 Algorithm

The iterative solver adjusts the auxiliary fluid inlet temperature of the heat exchanger until multiple conditions are met. This adjustment is carried out using the bisection

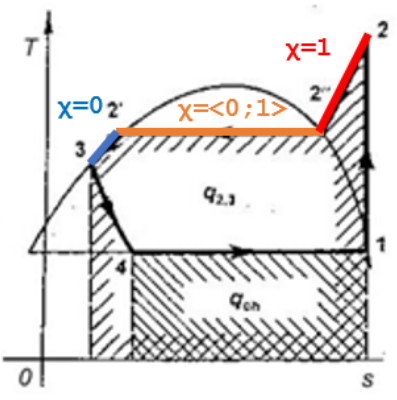

Figure 7: T-s diagram with vapour quality Nozicka (2008)

method, as described in Stepan (2012). Similar approaches have been implemented by Rice and Sand (1990), Admiraal and Bullard (1993), or Bansal and Purkayastha (1998). The first subsection of this chapter presents a simple heat exchanger model based on the implementation of *Ansys Fluent* Fluent (2009).
The second subsection of the chapter describes the proposed algorithm for calculating the AC condenser model, which has been developed in this thesis.
This model combines the single-phase and dual-phase heat exchanger (HTX) models based on input data and refrigerant characteristics, as shown in the T-s diagram shown in Figure 7 Nozicka (2008).
The AC condenser model iteratively determines the refrigerant subcooling, phase-change, and overcooling regions based on prescribed boundary conditions. It applies the appropriate $\epsilon - NTU$ relation and utilizes the measured $Q - Table$ for each region, as described in Section 3.

5 Measurement Devices

The selection of devices used for the measurements should align with the requirements for gathering input data for the $Q - Table$ as well as for verification measurements. This section describes the developed test bench, including sensor specifications, and provides a description of the tested AC condenser.
It is important to note that in the case of industrial applications, the test procedure needs to be fine-tuned to achieve more accurate and repeatable results. Additionally, the test setup should be capable of operating under a wider range of conditions to meet the requirements of industrial applications.

5.1 Test Equipment

The test equipment schematic is presented in Figure 9, showing a typical automotive AC thermodynamic circuit (Figure 8 Nozicka (2008)). The test equipment consists of three distinct and separate sections. The first section encompasses the refrigerant circuit, which includes the tested AC condenser (highlighted in red), evaporator, compressor, and thermal expansion valve. Pressure sensors and a flow meter are integrated within the refrigerant circuit for measurement purposes. The Figure 10 illustrates the test equipment, highlighting specific labeled components.
The second section pertains to the air side of the AC condenser, where cooling air is sucked into the AC condenser by an axial fan. This section represents the surrounding air of a vehicle or engine bay. To ensure a uniform flow throughout the AC condenser, the fan is positioned within a straight ducting configuration. Achieving flow uniformity is crucial for accurately measuring the performance of the heat exchanger ($Q - Table$), which serves as a crucial input for the developed model (Section 3).
The third section is physically separated and encompasses an evaporator, heater, and axial fan, representing the vehicle cabin.

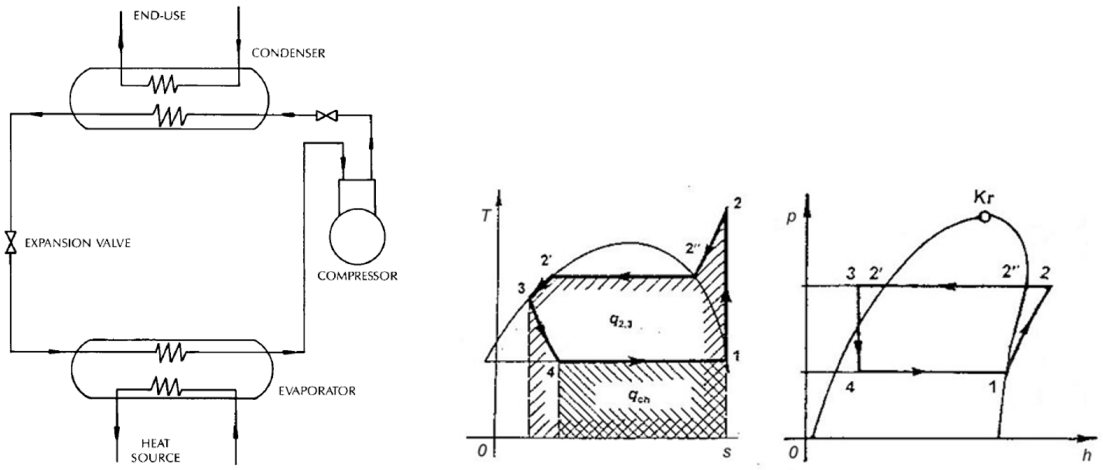

Figure 8: Function (a) Parise (1986) and thermodynamic scheme (b) of reverse ideal Rankine Cycle Nozicka (2008)

5.2 Sensor and Probes

The following list provides the measurement devices along with their respective systematic errors as provided by the manufacturers and data sampling frequencies.

- **Refrigerant flow**
  Flowmeter KROHNE DK34
  Maximum flow (kg/h) error of measured value is 4%
  Continuous measurement

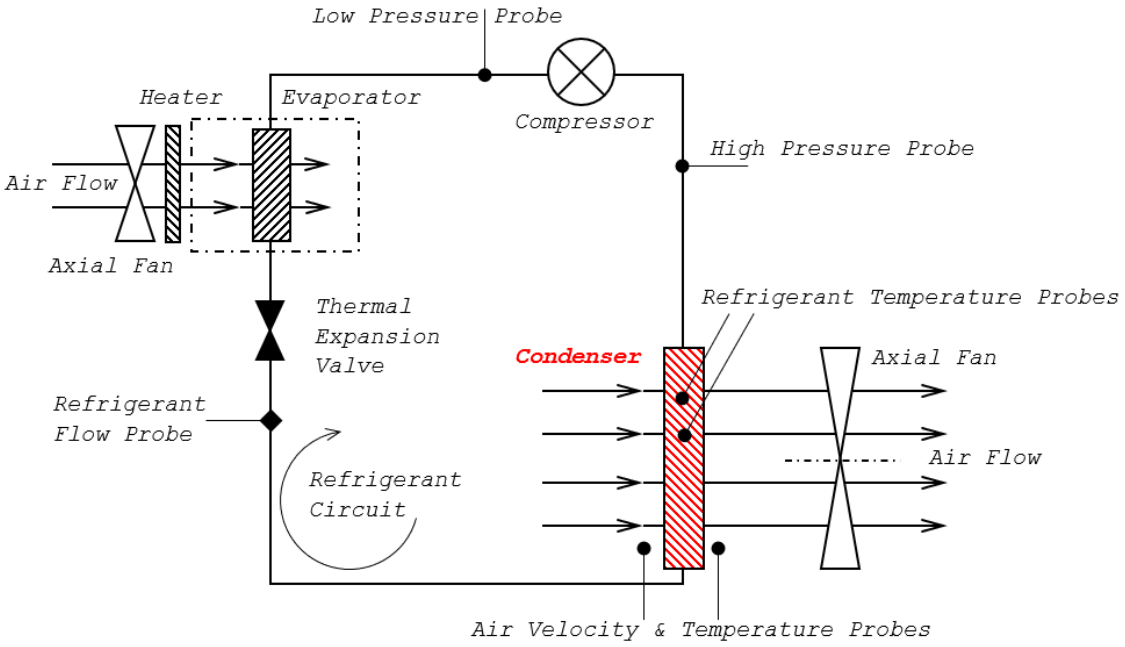

Figure 9: Test equipment scheme

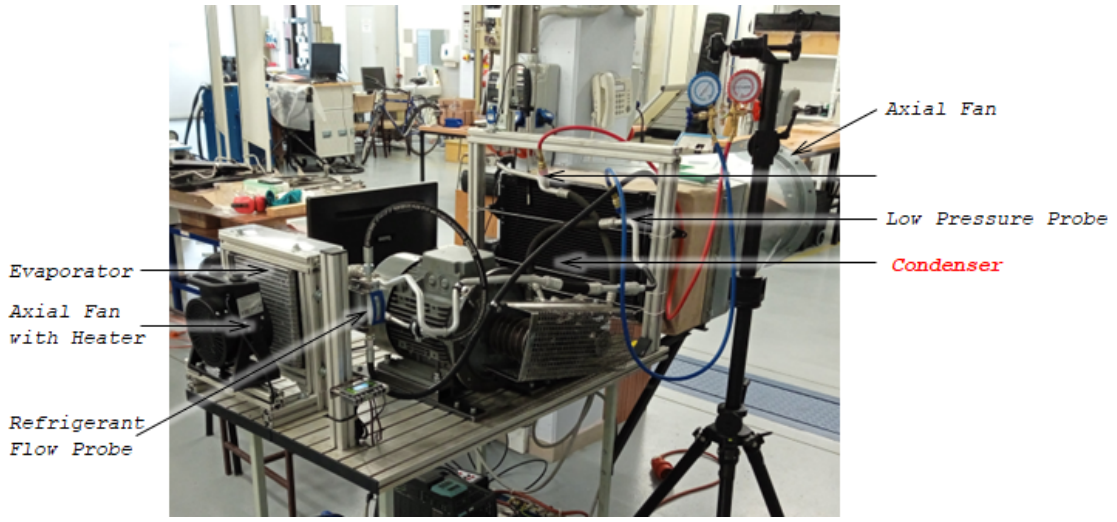

Figure 10: Test equipment photo

- **Refrigerant pressure**
  Manometer CT-466
  Maximum pressure (Psi) measuring error of measured value is 1.6% of span
  Continuous measurement

- **Air Flow**
  Anemometer VOLTCRAFT PL-135
  Maximum velocity (m/s) measuring error of measured value is $5\% + 0.01$
  Maximum temperature ($°C$) measuring error of measured value is $\pm 1°C$
  Sampling frequency 1Hz

- **Refrigerant and air temperature**
  Thermocouple OMEGA HH309A with grade K
  Maximum temperature ($°C$) measuring error of measured value is $\pm 1°C$
  Sampling frequency 1Hz

- **Refrigerant temperature**
  Thermal camera Testo 875
  Maximum temperature ($°C$) measuring error of measured value is $\pm 2°C$
  Continuous measurement

5.3 Tested AC Condenser

The evaluated AC condenser is originally used in Skoda Auto Roomster passenger vehicle. The AC condenser basic dimensions as well as passes division are shown in Figure 11 below. The AC condenser core thickness is $160mm$.

5.4 Refrigerant

The test equipment refrigerant circuit (Figure 9) is filled with R13a refrigerant. Detailed chemical specifications and material properties of the used refrigerant could be found in Morrison and Ward (1991). The R134a refrigerant properties described by an empirical function could be found in Oliveira and Wakeham (1993) or in the book of Poling et al. (2001).

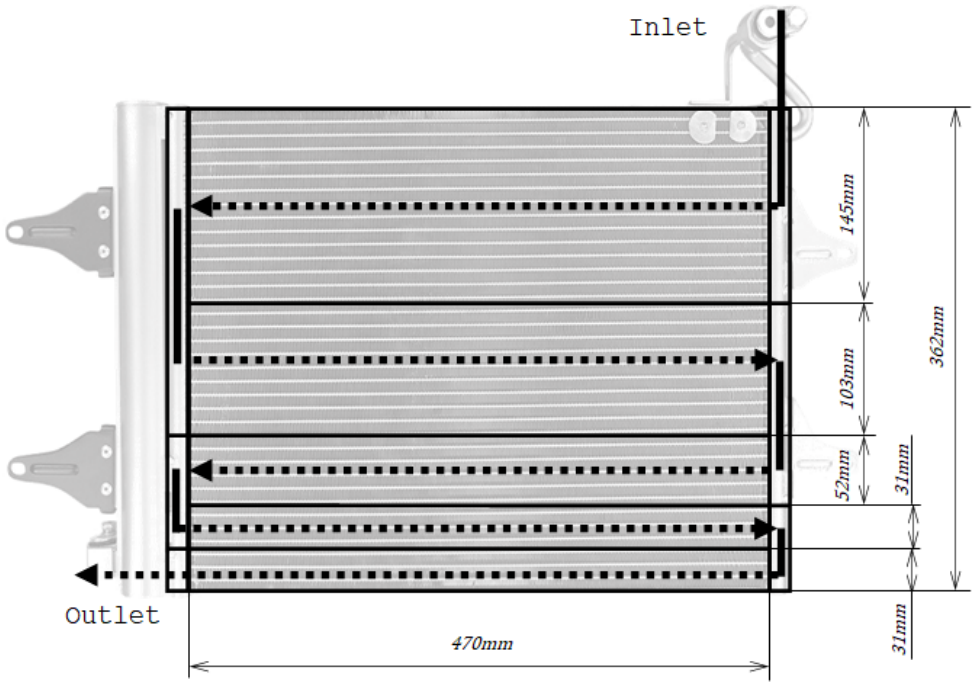

Figure 11: Evaluated AC condenser

6 Results

In order to validate the proposed AC condenser model that has been developed, two separate sets of measurements were conducted, referred to as Set A and Set B. Each set of measurements was carried out under distinct but constant and steady-state conditions and repeated tree times. For each measurement set, the model's input data ($Q-Table$), model boundary conditions, and verification data were recorded. This comprehensive approach eliminates the need for interpolating characteristic data ($Q-Table$) for various refrigerants and airflow rates, a requirement that may arise in industrial applications.

6.1 Air Flow Measurement

The airflow measurement provides the input data for the AC condenser model as well as verification data. For the input, the model uses the airflow inlet velocity and temperature, while for model verification, the air outlet temperatures. The model aims to accurately predict the air outlet temperatures based on the given inlet velocity and temperature.

6.1.1 Air Flow Inlet

The measurement of airflow inlet serves as the boundary condition for the developed AC condenser model, specifically determining the air inlet mass flow rate and temperature. The direct measurement of air mass flow rate is not performed; instead, it is calculated based on the magnitude of air velocity using the equation 3 Nozicka (2008). Addition-

ally, the airflow measurement is utilized to determine the characteristic data of the AC condenser.

Table 1 and 2 present the results of the first set (Set A) of air flow inlet measurements, accompanied by the corresponding uncertainties. The average inlet velocity is calculated to be $1.669 m/s$ with a uniformity index of 0.982. The average inlet air temperature is $24.42°C$ with a uniformity index of 0.999.

Similarly, Table 3 and 4 present the results of the second set (Set B) of air flow inlet measurements, along with the corresponding uncertainties. The average inlet velocity for this set is determined to be $1.265 m/s$ m/s, with a uniformity index of 0.977. The average inlet air temperature is recorded as $18.23°C$, with a uniformity index of 0.999.

The mean refers to the area-weighted average for both quantities and for both measurement sets. The uniformity index is relatively high, which is crucial for the characteristic data measurement results in the next Section 6.2.

Table 1: Air inlet velocity measurement Set A

Air inlet velocity (m/s)					
Loc.	A	B	C	D	E
1	1.599±0.101	1.625±0.187	1.627±0.141	1.622±0.152	1.570±0.101
2	1.761±0.107	1.767±0.140	1.680±0.175	1.721±0.133	1.695±0.172
3	1.757±0.115	1.604±0.101	1.699±0.106	1.695±0.140	1.700±0.146
4	1.768±0.244	1.696±0.128	1.567±0.142	1.792±0.122	1.648±0.160
5	1.573±0.169	1.583±0.109	1.657±0.177	1.726±0.138	1.593±0.131

Table 2: Air inlet temperature measurement Set A

Air inlet temperature (°C)					
Loc.	A	B	C	D	E
1	24.245±1.016	24.392±1.012	24.203±1.040	24.746±1.196	24.635±1.076
2	23.900±1.014	24.100±1.027	25.126±1.920	25.432±1.089	24.999±1.046
3	23.876±1.014	24.040±1.013	24.559±1.145	24.445±1.051	25.026±1.081
4	23.869±1.066	23.802±1.010	24.393±1.046	24.345±1.072	25.700±1.175
5	23.657±1.057	23.452±1.021	23.816±1.063	24.069±1.149	25.683±1.183

Table 3: Air inlet velocity measurement Set B

Air inlet velocity (m/s)					
Loc.	A	B	C	D	E
1	1.143±0.085	1.288±0.171	1.280±0.089	1.122±0.087	1.139±0.109
2	1.325±0.126	1.193±0.130	1.240±0.099	1.136±0.104	1.270±0.130
3	1.239±0.114	1.209±0.136	1.267±0.099	1.292±0.126	1.315±0.127
4	1.311±0.093	1.328±0.087	1.263±0.097	1.337±0.098	1.352±0.090
5	1.387±0.082	1.338±0.141	1.239±0.101	1.276±0.090	1.324±0.094

Table 4: Air inlet temperature measurement Set B

Air inlet temperature (°C)					
Loc.	A	B	C	D	E
1	18.215±1.157	18.244±1.009	18.154±1.007	18.502±1.008	18.517±1.045
2	17.484±1.106	18.079±1.077	18.480±1.036	18.853±1.030	18.856±1.045
3	17.399±1.000	17.730±1.026	18.262±1.026	18.881±1.061	19.101±1.032
4	17.312±1.012	17.438±1.012	18.408±1.009	18.541±1.052	19.006±1.047
5	17.073±1.014	17.421±1.053	18.612±1.071	18.533±1.050	19.209±1.036

6.1.2 Air Flow Outlet

The air outlet temperature measurements for Sets A and B are listed in Tables 5 and 6, respectively. The corresponding uncertainties are provided within the tabels.

Table 5: Air outlet temperature measurement Set A

Air outlet temperature (°C)					
Loc.	A	B	C	D	E
1	37.246±1.065	28.359±1.075	28.795±1.036	29.702±1.377	29.394±1.102
2	36.726±1.032	29.243±1.012	28.474±1.305	29.350±1.032	28.835±1.249
3	29.239±1.125	28.596±1.272	27.777±1.024	29.220±1.105	27.979±1.489
4	29.685±1.009	28.850±1.031	27.783±1.070	29.094±1.321	28.085±1.279
5	29.485±1.011	29.400±1.187	28.389±1.038	28.863±1.358	28.652±1.401

Table 6: Air outlet temperature measurement Set B

Air outlet temperature (°C)					
Loc.	A	B	C	D	E
1	28.921±1.059	25.510±1.027	25.523±1.027	25.456±1.089	25.815±1.047
2	29.047±1.034	25.778±1.071	25.509±1.088	25.719±1.037	25.862±1.036
3	25.872±1.058	25.259±1.044	25.584±1.020	25.839±1.131	25.881±1.205
4	25.492±1.052	25.671±1.165	25.304±1.029	25.686±1.080	25.915±1.045
5	25.352±1.068	25.637±1.034	25.631±1.060	25.702±1.046	25.647±1.204

6.2 Characteristic Data Measurement

The measurement of characteristic data provides vital information on various parameters, including the refrigerant mass flow rate, refrigerant inlet pressure, and refrigerant inlet and outlet temperatures, for both Set A and Set B measurements. Furthermore, the frontal area for each phase is measured. This allows for the acquisition of essential input data for equation 10 Fluent (2009), which is utilized in the developed AC condenser model.
In Set A, the measured refrigerant mass flow rate is determined to be $0.018 + / - 0.001(kg/s)$, with a measurement uncertainty of 4.038% relative to the mass flow rate value. The refrigerant AC condenser inlet and outlet temperatures are recorded as

$40.626 + / - 1.291°C$) and $27.684 + / - 1.272°C$, respectively. The refrigerant inlet pressure is measured at $105.2 + / - 8.010(psi)$, with a measurement uncertainty of 7.031% relative to the pressure value.

In Set B, the measured refrigerant mass flow rate is determined to be $0.015 + / - 0.001(kg/s)$, with a measurement uncertainty of 4.031% relative to the mass flow rate value. The refrigerant AC condenser inlet and outlet temperatures are recorded as $29.190 + / - 1.242°C$ and $24.637 + / - 1.154°C$, respectively. The refrigerant inlet pressure is measured at $90.267 + / - 8.001(psi)$, with a measurement uncertainty of 7.614% relative to the pressure value.

The temperature measurement curves are shown for the both measurement sets in the Figure 12. The time development of these curves serves as evidence of the steady-state conditions within the measurements.

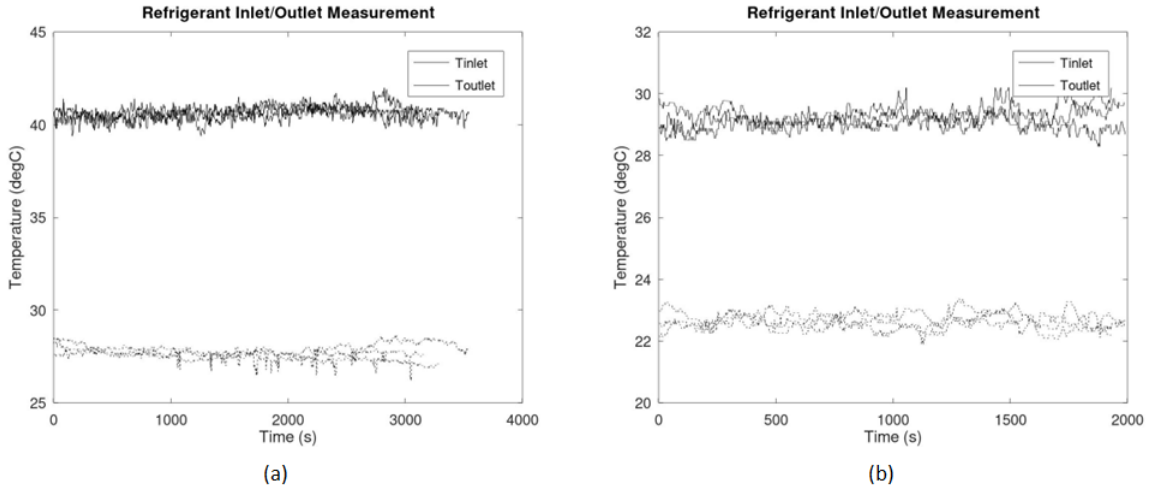

Figure 12: Refrigerant inlet and outlet temperature (°C) (a) Set A; (b) Set B

Based on the aforementioned measured values, the heat release for each refrigerant section, as well as the overall heat dissipation, is calculated. The heat dissipation values on the refrigerant side are presented in the Table 7. It is important to note that the accuracy of measuring the total heat dissipation within the AC condenser is 16.441% for Set A measurements and 27.653% for Set B. As indicated in Table 7, both measurements did not reach the overcooling section (liquid section). The inability to measure the overcooling section is attributed to the refrigerant saturated temperature falling within the uncertainties of the refrigerant outlet measurements. However, achieving overcooling in the AC condenser can be accomplished in a integrated dryer connected to the AC condenser's refrigerant outlet.

The calculation of heat dissipation on the air side is performed using Equation 5 Incropera et al. (2011), along with the measured values of airflow from Section 6.1. The obtained results are presented in Table 8.

Table 7: Measured heat dissipation on refrigerant side

Heat dissipation (W)		
Region	Set A	Set B
Gas	247.382 +/-32.893	98.187 +/-22.030
Dual	3175.714 +/-21.321	2712.147 +/-9.561
Liquid	N/A	N/A
Overall	3423.096 +/-562.792	2810.334 +/-777.127

Table 8: Measured heat dissipation on air side

Heat dissipation (W)		
Region	Set A	Set B
Gas	327.632 +/-20.068	268.357 +/-20.636
Dual	1362.951 +/-16.860	1737.456 +/-17.315
Liquid	N/A	N/A
Overall	1690.583 +/-16.876	2005.813 +/-17.308

The refrigerant state (gas, dual-phase and liquid) regions size for measurement Set A and Set B are specified in Table 9.

Table 9: Refrigerant state region areas

Area (m^2)		
Region	Set A	Set B
Gas	0.010	0.007
Dual	0.160	0.163
Liquid	N/A	N/A

Table 10 represents the combined heat dissipation, in terms of statistical combination of measured values on refrigerant and air side. Regarding the higher uncertainty in the heat dissipation on the refrigerant side compared to the air side, the combined heat dissipation aligns more closely with the refrigerant side. However, it's important to note that the uncertainty in the air side does not account for the sensitivity to the number of measured points in Figure 13. This aspect should be further investigated, especially in the case of industrial applications. The combined heat dissipation value should be applied in the setup of the AC condenser model. However, the refrigerant side heat dissipation could be preferred over the combined or air heat dissipation due to the inherent uncertainties associated with the number of measured points in the air side.

6.3 Verification Measurement

The model's verification is performed via comparing the results of the AC condenser model with the measured air outlet temperature (Section 6.1.2) and the refrigerant inlet and outlet temperature (Section 6.2)

Table 10: Measured heat dissipation

Heat dissipation (W)		
Region	Set A	Set B
Gas	269.150 +/-24.725	177.718 +/-20.801
Dual	2478.280 +/-20.627	1965.202 +/-11.817
Liquid	N/A	N/A
Overall	3421.540 +/-455.746	2809.935 +/-520.697

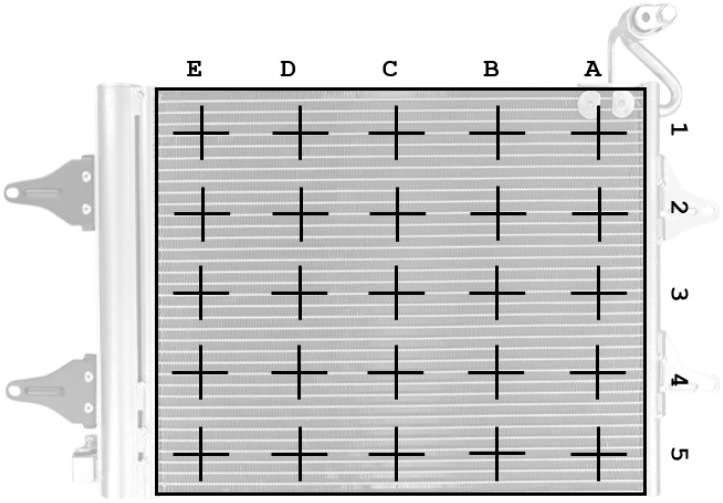

Figure 13: Measurement locations

6.4 AC Condenser Model

The computational domain, as shown in Figure 3, has been discretized into a numerical grid consisting of $(8, 75, 35)$ cells along the coordinate system. The size of the domain has been determined based on the dimensions of the evaluated AC condenser (Figure 11).
The mesh size was chosen following a mesh sensitivity study, as illustrated in Figure 14. The plot shows the resulting auxiliary inlet temperature against the cell count. The highlighted mesh size is selected , as further increasing the mesh decomposition does not significantly affects the results.
The boundary condition for the air inlet mass flow rate is determined using air flow velocity and temperature measurements, as described in Section 4.2.1, and utilizing data from Section 6.1.1. For both setup Sets A and B, constant material properties were defined based on appropriate average temperature or measured pressure,. In both calculations, the convergence tolerance δ was set to $1W$. The convergence of overall heat dissipation in setup Set A and Set B during the solution process is illustrated in Figure 15. The upper limit for the bisection method was established at $200K$ above the saturated temperature, specific to each respective Set.
The characteristic data and heat dissipation values for the entire AC condenser are derived from the findings presented in Section 6.2. Specifically, Table 7 provides the relevant infor-

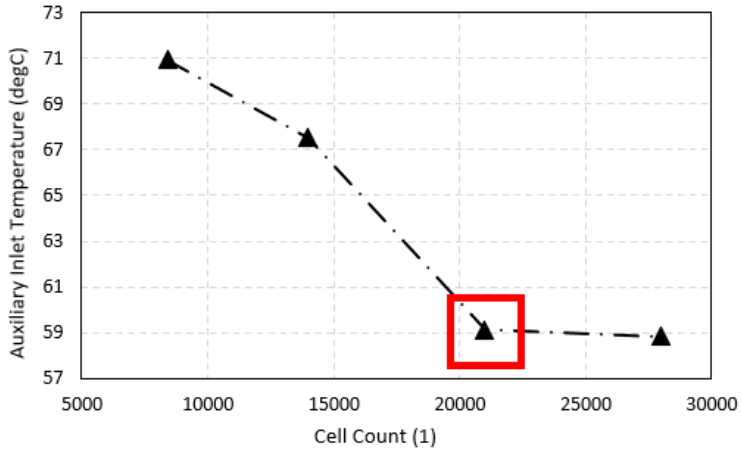

Figure 14: Mesh sensitivity study

mation. This table was preferred over Table 10 because the uncertainty of the dissipation on the air side is affected by the spatial distribution of measured points, a parameter that was not determined in this thesis. Therefore, further investigation is required to address this aspect. Nevertheless, the difference between the refrigerant side and the combined heat dissipation is negligible for the both measurements sets.

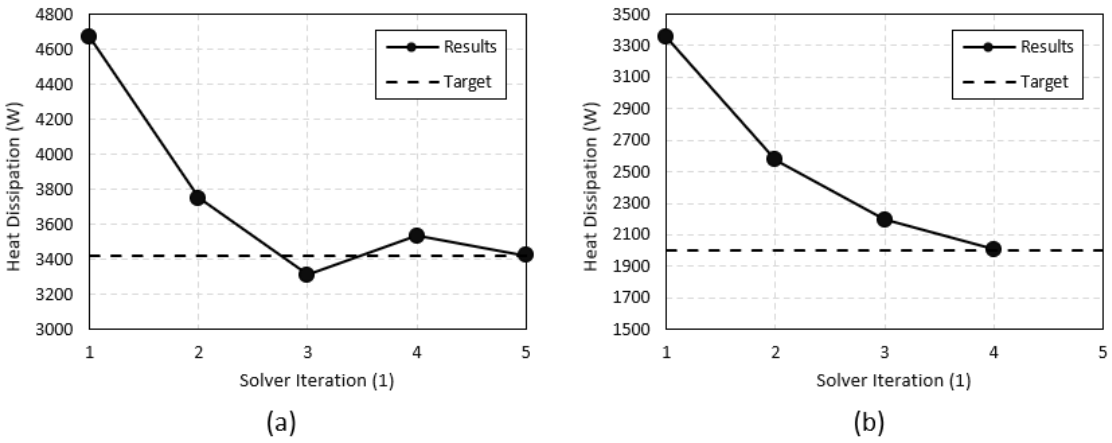

Figure 15: Convergence (a) Set A; (b) Set B

The contour plots displaying the resultant air outlet temperature for both setup Sets A and B, are presented in Figures 16. The refrigerant inlet and outlet temperatures are 60.884°C and 27.876°C, respectively, for Set A, while for Set B, the corresponding values are 41.793°C and 23.043°C. The refrigerant temperature contour is shown in Figure 17. The model results show a significant tendency to overpredict the verification measurements (Section 6.3). However, it is important to acknowledge that the input data, especially concerning heat dissipation, exhibits relatively high uncertainty. This uncertainty allows for adjustments to the input parameters, enabling the model to align better with the measured values.

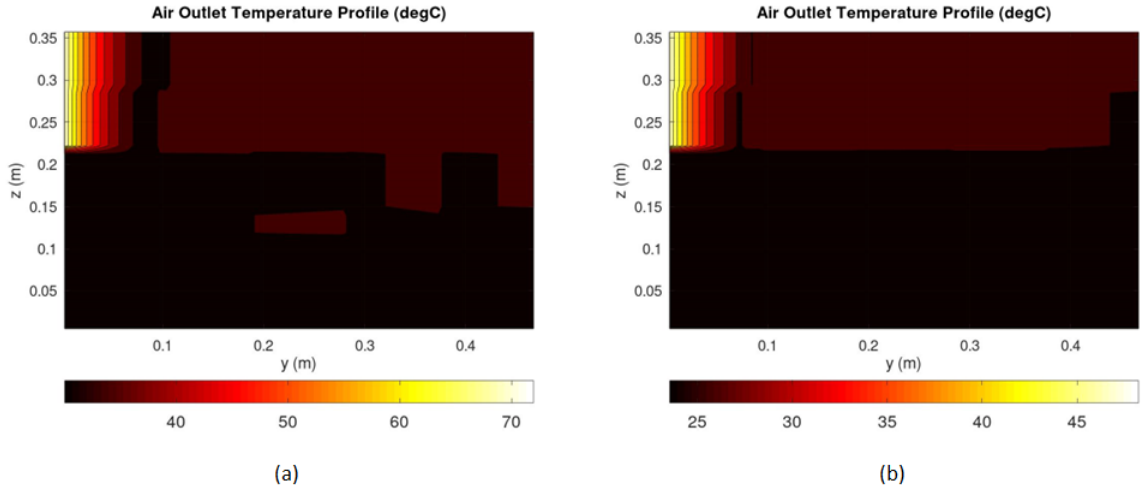

Figure 16: Air outlet temperature (°C) (a) Set A; (b) Set B

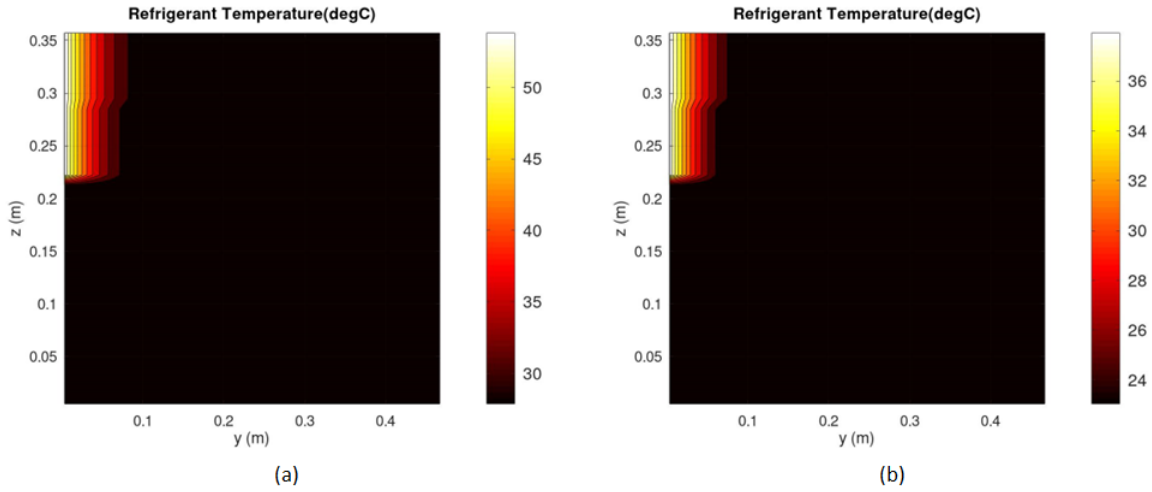

Figure 17: Refrigerant temperature (°C) (a) Set A; (b) Set B

7 Conclusions

Within the thesis, a comprehensive study of AC condenser heat transfer modeling and measurement was conducted. The primary focus was on developing a simplified model suitable for complex 3D computational fluid dynamics (CFD) simulations.

The philosophy underlying the suggested model is to iteratively utilize directly measured overall heat transfer coefficients instead of relying on literature or separately measured convective/condensation heat transfer coefficients. These separately measured coefficients are specific to the micro-channel heat exchanger design, the refrigerant used, and the operating conditions. Thus, the proposed approach offers greater generality while significantly reducing the amount of required input information. However, it should be noted that this approach necessitates the modification of input data measurements.

The developed model utilized the widely recognized $\epsilon - NTU$ approach, as elaborated in Section 3. Through this approach, the AC condenser model iteratively predicts locally refrigerant phase and appropriately selects heat transfer models and measured characteristics, resulting in an accurate spatial distribution of heat dissipation. Enhanced predictions of refrigerant and air temperatures generally lead to improved predictions of other components within a vehicle. This is particularly advantageous, especially for battery electric vehicles (BEVs), where the requirements for thermal management are becoming increasingly stringent. In the context of BEVs, every watt of energy must be carefully considered and efficiently managed to optimize the performance and range of the vehicle.

In Section 6.4, the suggested and developed model's results for the refrigerant inlet temperature were found to exhibit significant over-prediction. For Set A, the model over-predicted the refrigerant temperature by more than $18.967K$, while for Set B, the over-prediction was above $12.603K$. Consequently, the air outlet temperature was also over-predicted.

However, when the input heat dissipation was reduced by 8% for Set A and by 7% for Set B, the resulting refrigerant inlet temperature fell within the uncertainty bounds of the measurement data, as shown in Figure 18. Similarly, the refrigerant outlet temperatures of $27.876°C$ for Set A and $23.043°C$ for Set B were also within the uncertainty range of the corresponding measurements, which were $27.684 \pm 1.272°C$ and $22.637 \pm 1.154°C$, respectively.

The reduced prescribed heat dissipation is within the range of uncertainty for the measured heat dissipation (Table 7), the model achieved improved agreement also with the measured air outlet temperatures. The contours of the air outlet temperature with the reduced heat dissipation prescribed in the model are shown in Figure 19, and a comparison with the measurement data is presented in Figures 20, 21, 22, 23, and 24. It was observed that the predicted values were in good agreement with the measurement data for Set B, while in Set A, there was a slight over-prediction.

One noteworthy observation in Figure 20 was a significant change in the air outlet temperature, highlighted by a red box. This change was attributed to the refrigerant being cooled to the saturation temperature, altering the heat transfer behavior.
Overall, the findings highlighted the sensitivity of the model to the prescribed heat dissipation and its ability to match the measurement data when within the range of uncertainty. The results presented in the thesis demonstrate the feasibility of the developed AC condenser model and measurement approach for industrial application, while keeping the aforementioned benefits.

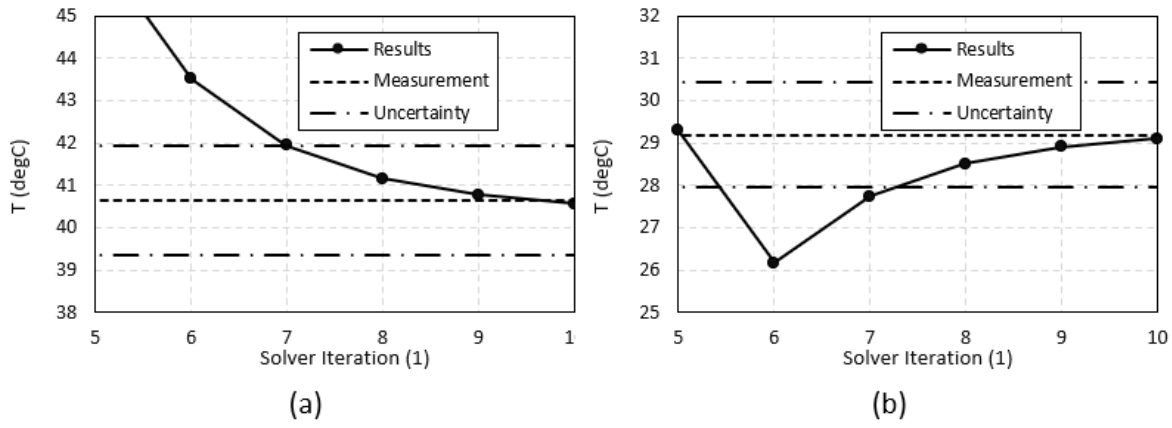

Figure 18: Refrigerant inlet temperature (°C) (a) Set A ; (b) Set B

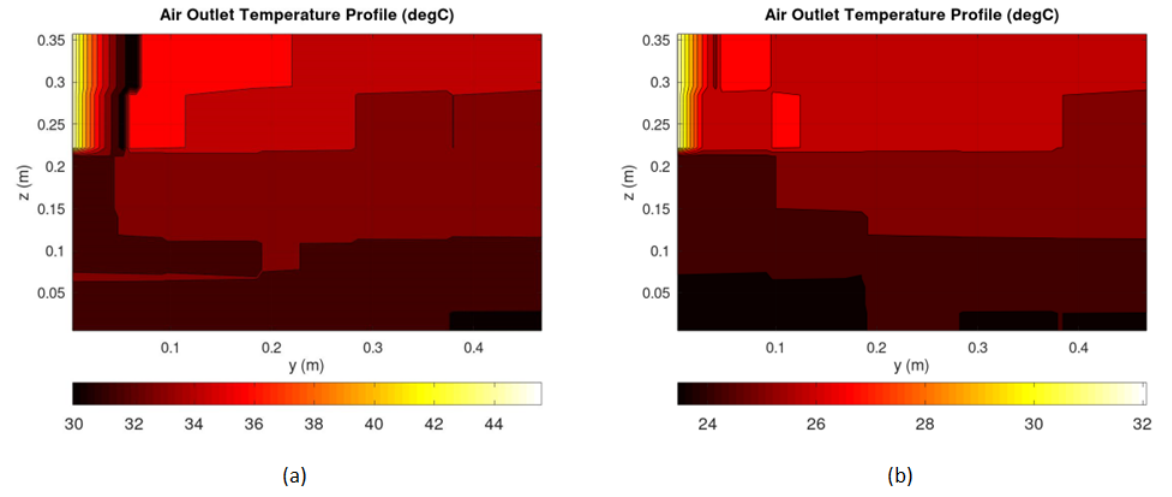

Figure 19: Air outlet temperature (°C) (a) Set A; (b) Set B

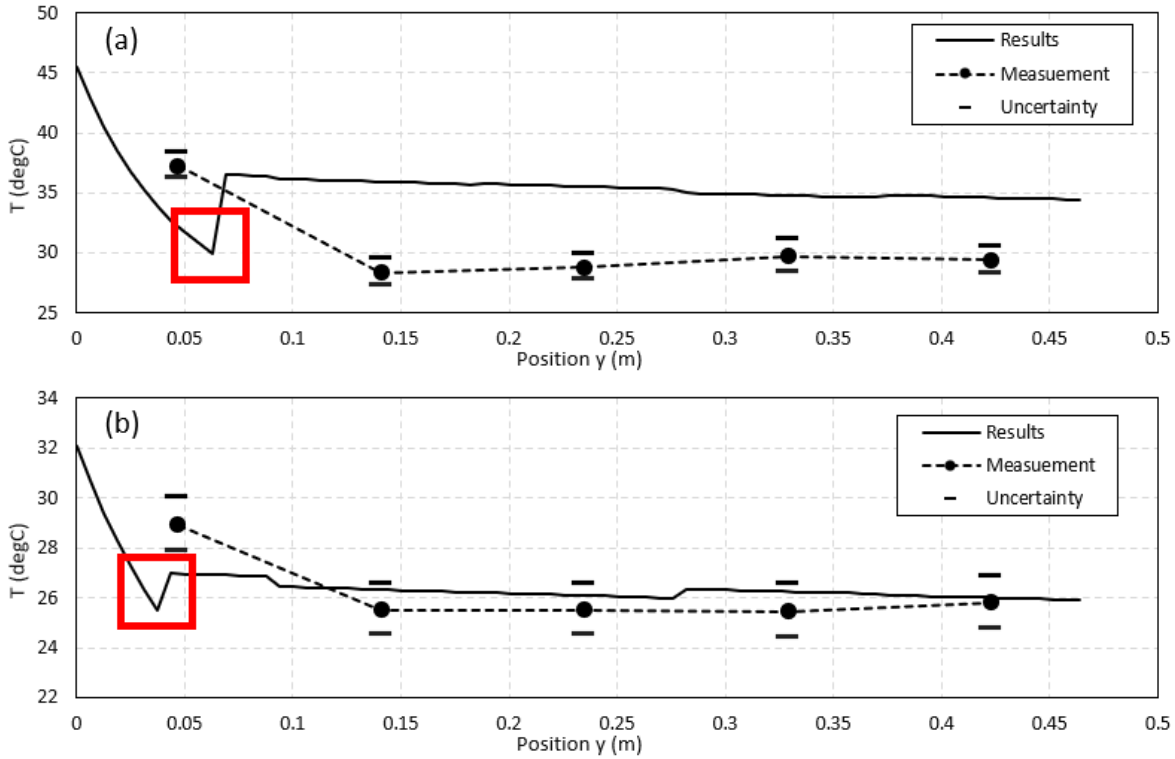

Figure 20: Air outlet temperature A1;B1;C1;D1;E1 (°C) (a) Set A; (b) Set B

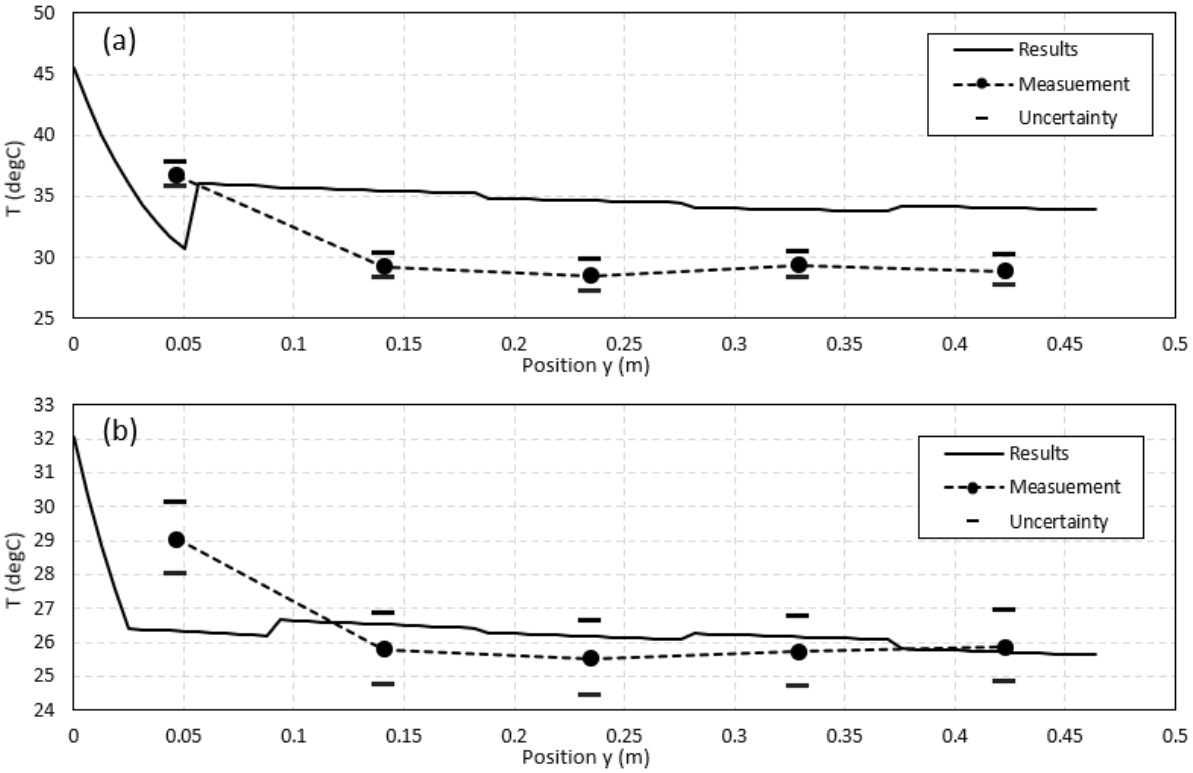

Figure 21: Air outlet temperature A2;B2;C2;D2;E2 (°C) (a) Set A; (b) Set B

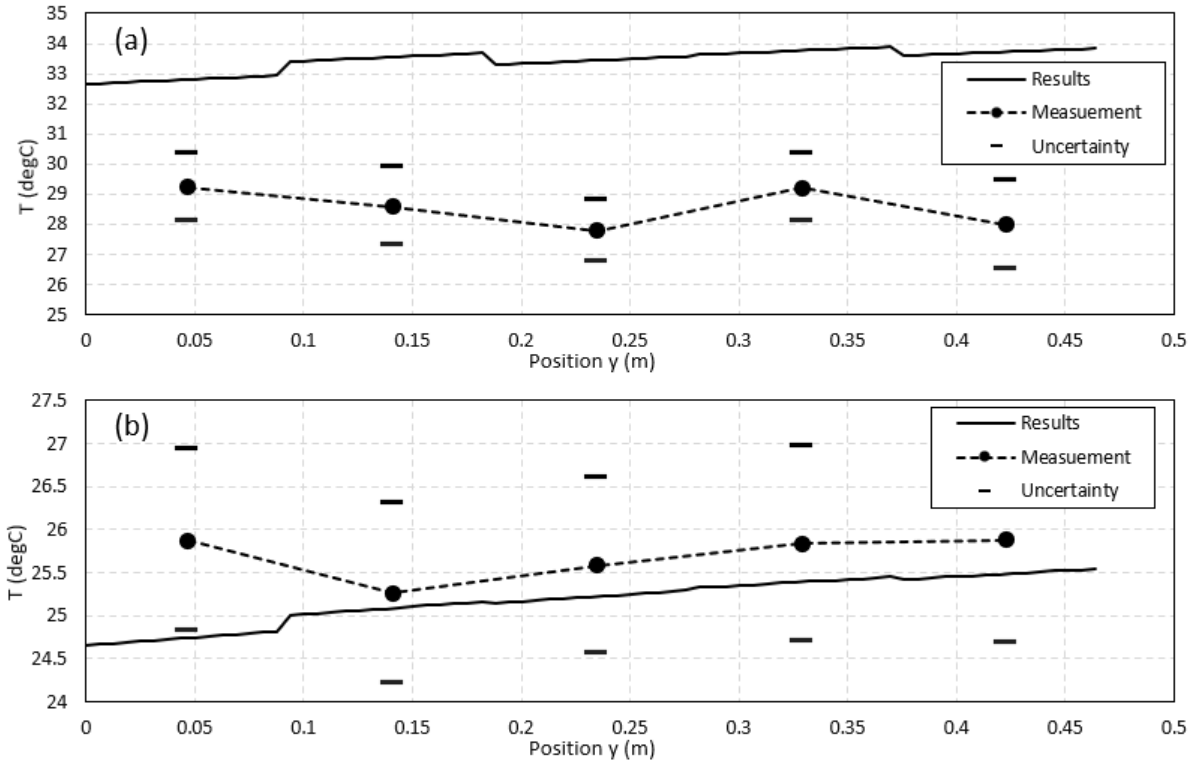

Figure 22: Air outlet temperature A3;B3;C3;D3;E3 (°C) (a) Set A; (b) Set B

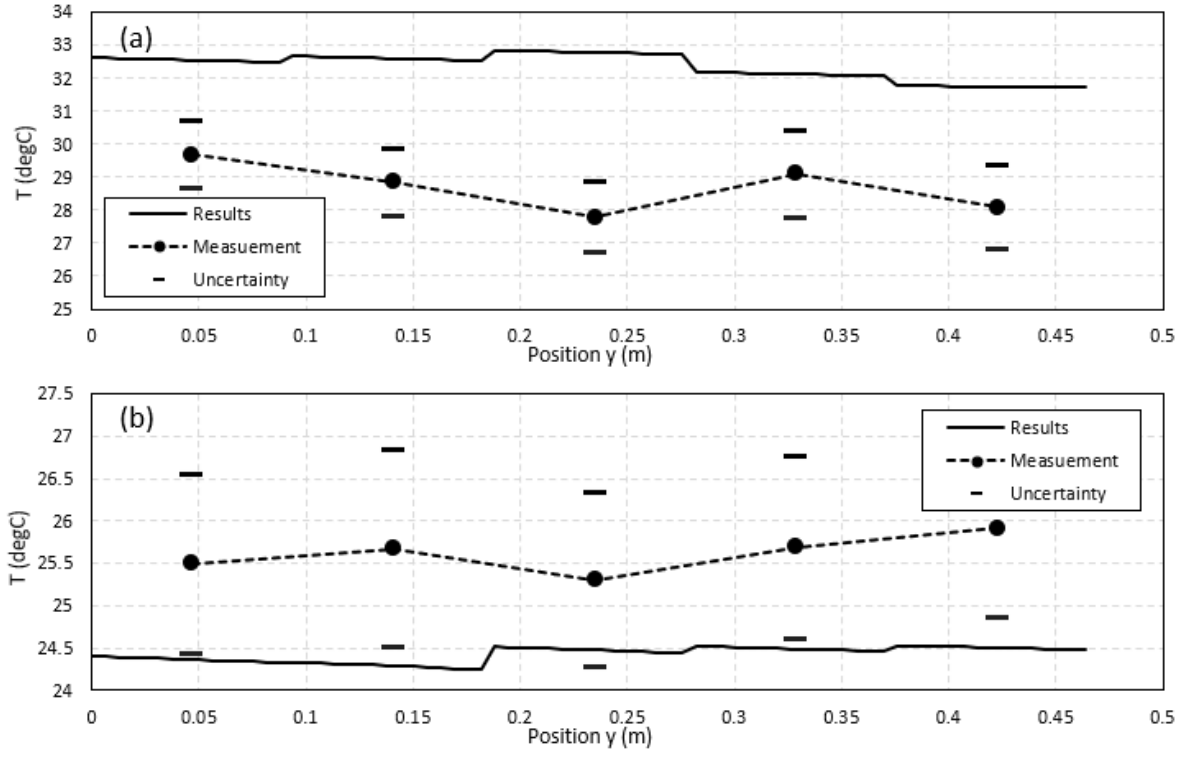

Figure 23: Air outlet temperature A4;B4;C4;D4;E4 (°C) (a) Set A; (b) Set B

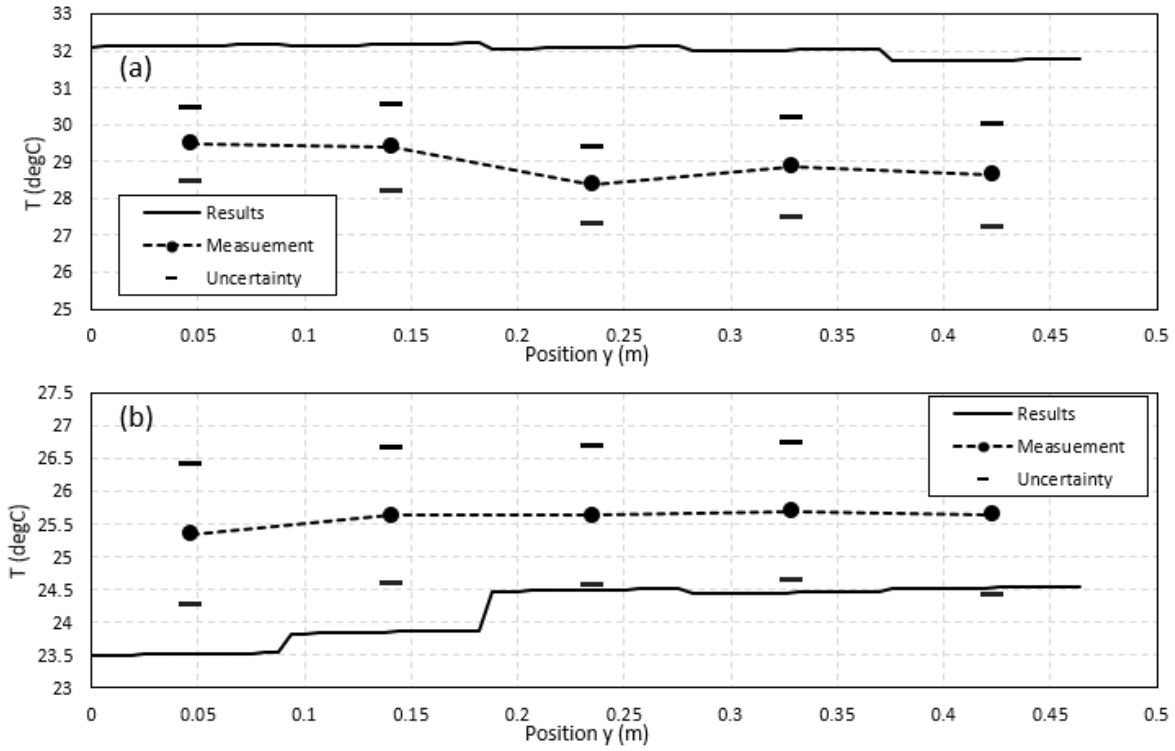

Figure 24: Air outlet temperature A5;B5;C5;D5;E5 (°C) (a) Set A; (b) Set B

7.1 Future Research

As discussed in the results Section 6, further investigation is needed for model industrialization and validation. Key tasks include improving measurement accuracy by increasing measuring points on the air side, and enhancing temperature measurement precision as per standard EN1643033 (2011).

For industrial application, it is essential to measure more characteristic data and operating points to ensure comprehensive coverage of various scenarios. Additionally, coupling the model with 3D CFD and investigating its influence on the underhood compartments are crucial steps for evaluating the developed model impact.

Furthermore, it would be appropriate to conduct studies focusing on comparing the results of the developed model with other approaches under a wider range of operating conditions. With the aim of quantifying the model's limitations and benefits.

8 Contributions

First-author

Schmid, M. (2019). Windshield Defrost Simplified CFD Model. *Production Engineering Archives*, **25**(25), 8-11.

Schmid, M., Pascenko, P., Bozkurt, F. and Petrzela, P. (2021). Importance of three- dimensional vehicle heat exchanger modeling, *Journal of Thermal Science and Engi- neering Applications* **14**(7): 7

Schmid, M., Tomek, P., and Hanus, P. (2022). Multi-physical contact simulation in vehicle applications. *Production Engineering Archives*, **28**(4), 369-374.

Co-author

Schmidova, E., Bozkurt, F., Schmid, M., and Culek, B. (2016). LOCAL ELASTIC-PLASTIC RESPONSE OF WELDING JOINTS OF DOMEX700MS STEEL. *In METAL 2016: 25th International Conference on Metallurgy and Materials*. TANGER, spol. s ro.

Kaya, U., Schmidova, E., Schmid, M., and Culek, B. (2016). Rolling-Contact Hardening Evaluated by Indentation.*In Defect and Diffusion Forum*,(Vol. **2368**, pp. 11-14). Trans Tech Publications Ltd.

Schmidova, E., Hojka, P., Culek, B., Klejch, F., and Schmid, M. (2019). Dynamic strength and anisotropy of DMLS manufactured maraging steel. *Komunikacie: Communications (Scientific Letters of the University of Zilina)*, volume **21**, issue: 3.

Schmidova, E., Kumar, M. S., Schmid, M., and Bozkurt, F. (2020). Role of Nb in the failure of dual-phase steel in heterogeneous welds. *Engineering Failure Analysis*, **116**, 104708.

Pascenko, P., Schmidova, E., Culek, B., and Schmid, M. (2021). Premature failures of railway axles after repeated pressing. *Engineering Failure Analysis*, **123**, 105253.

Projects

Narodni centrum kompetence Josefa Bozka, č. TN 0100 0026; (2019-2022)

Eliminace provoznich poruch naprav kolejovych vozidel, projekt TACR, c. TH 02010542; (2017-2019)

Prediktivni udrzba kolejove dopravni cesty, DOPRAVA 2020+, č. CK02000177 (2021-2024)

Narodni centrum kompetence inzenyrstvi pozemnich vozidel Josefa Bozka, č. TN02000054 (2023-2028)

References

Admiraal, D. M. and Bullard, C. W. (1993). *Heat Transfer in Refrigerator Condensers and Evaporators*, University of Illinois.

Bansal, P. K. and Purkayastha, B. (1998). An ntu-e model for alternative refrigerants, *International Journal of Refrigeration* **21**(5): 381–397.

EN1643033 (2011). *Fan assisted radiators, convectors and trench convectors Part 3 Test method and rating of cooling capacity*, Standard.

Fluent, A. (2009). *Theory Guide Release 12.0*, Ansys.

Gamma Technologies, I. (2014). *GT-Suite User's Manual*, Gamma Technologies, Inc. Westmont IL.

Incropera, F. P., Dewitt, D. P., Bergman, T. L. and Lavine, A. S. (2011). *Fundamentals of Heat and Mass Transfer 7th edition*, John Wiley & Sons ISBN 13 978-0470-50197-9.

J902, S. (2011). *Surface Vehicle Recommended Practice*, SAE International.

Jha, K. K. and Shaik, I. (2016). Scaling model of heat exchangers in automotive air conditioning systems, *SAE Technical Paper* **No. 2016-01-0227**.

Kays, W. M. and London, A. L. (1984). *Compact Heat Exchangers 3th Edition*, Krieger Publishing Company, ISBN 1-57524-060-2.

König, A., Mayer, S., Nicoletti, L., Tumphart, S. and Lienkamp, M. (2022). The impact of hvac on the development of autonomous and electric vehicle concepts, *Energies* **15**: 441.

Liang, Y. Y., Liu, C. C., Li, C. Z. and Chen, J. P. (2015). Experimental and simulation study on the air side thermal hydraulic performance of automotive heat exchangers, *Applied Thermal Engineering* **87**: 305–315.

Minqiang, P. A. N., Dehuai, Z., Yong, T. and Dongqing, C. (2009). Cfd-based study of velocity distribution among multiple parallel microchannels, *Journal of Computers* **4**(11): 1133–1138.

Mohammadi, M., Jovanovic, G. N. and Sharp, K. V. (2013). Numerical study of flow uniformity and pressure characteristics within a microchannel array with triangular manifolds, *Computers & Chemical Engineering* **52**: 134–144.

Moradi, I., Arash, K., Masoud, A., Zhixiong, L. and Quang-Vu, B. (2020). Three-dimensional numerical simulation of external fluid flow and heat transfer of a heat exchanger in a wind tunnel using porous media mode, *Journal of Thermal Analysis and Calorimetry* **141**(5): 1647–1667.

Morrison, G. and Ward, D. K. (1991). Thermodynamic properties of two alternative refrigerants: 1, 1-dichloro-2, 2, 2-trifluoroethane (r123) and 1, 1, 1, 2-tetrafluoroethane (r134a), *Fluid Phase Equilibria* **62**(1-2): 65–86.

Nozicka, J. (2008). *Zaklady Termomechanicky*, Ceska technika - nakladatelstvi CVUT.

Oliveira, C. M. B. P. and Wakeham, W. A. (1993). The viscosity of liquid r134a, *International journal of thermophysics* **14**: 33–44.

Parise, J. A. R. (1986). Simulation of vapour-compression heat pumps, *Simulation* **46**(2): 71–76.

Pervaiz, M. M., Brewster, R. A., Ross, F., Bauer, W. and Reister, H. (1997). Numerical methodology for automotive radiator and condenser simulations, *SAE Transactions JOURNAL OF PASSENGER CARS* pp. 2475–2501.

Pistoresi, C., Fan, Y. and Luo, L. (2015). Numerical study on the improvement of flow distribution uniformity among parallel mini-channels, *Chemical Engineering and Processing: Process Intensification* **95**: 63–71.

Poling, B. E., Prausnitz, J. M. and O'Connell, J. P. (2001). *The properties of gases and liquids*, McGraw-Hill Education.

Rice, C. K. and Sand, J. B. (1990). Initial parametric results using cycles an lmtd-specified, lorenz-meutzner cycle refrigerator-freezer model, *International Refrigeration and Air Conditioning Conference* **CONF-900742-1**: 130.

Schmid, M., Pascenko, P., Bozkurt, F. and Petrzela, P. (2021). Importance of three-dimensional vehicle heat exchanger modeling, *Journal of Thermal Science and Engineering Applications* **14**(7): 7.

Stepan, B. D. G. (2012). Bisection method in higher dimensions and the efficiency number, *Periodica Polytechnica Mechanical Engineering* **56**(2): 81–86.

Taborek, J. (1983). *Handbook of Heat Exchanger Design*, Hemisphere.

Wei, M., Fan, Y., Luo, L. and Flamant, G. (2015). Cfd-based evolutionary algorithm for the realization of target fluid flow distribution among parallel channels, *Chemical Engineering Research and Design* **100**: 341–352.

Zou, Y. and Hrnjak, P. S. (2014). Effects of fluid properties on two-phase flow and refrigerant distribution in the vertical header of a reversible microchannel heat exchanger–comparing r245fa, r134a, r410a, and r32, *Applied Thermal Engineering* **70**(1): 966–976.